Particle collisions control stable bed configuration under weak bedload transport conditions

Thomas C. Ashley[1], **Suleyman Naqshband**[2], **Brandon McElroy**[1]

[1]Department of Geology and Geophysics, University of Wyoming, Laramie, WY
[2]Department of Environmental Sciences, Wageningen University, Wageningen, Netherlands

Key Points:

- Experiments highlight differences in particle behavior over stable and unstable planar topography.
- Planar topography is unstable when particle collision events are more frequent than entrainment events.
- A theoretical stability field for lower-stage plane bed topography is proposed.

Corresponding author: Thomas C. Ashley, `tashley22@gmail.com`

Abstract

Sedimentary bed configurations that are stable under weak fluid-driven transport conditions can be divided into two groups: (1) meso-scale features that influence flow and sediment transport through roughness and drag partitioning effects ("mesoforms"), and (2) grain-scale features that can effectively be ignored at the macroscopic scale ("microforms"). In practice, these groups delineate ripples and dunes from quasi-planar bed configurations. They are thought to be separated by a transition in processes governing the relief of the bed; however, the physical mechanisms responsible for this transition are poorly understood. Previous studies suggest that planar topography is unstable when interactions between moving particles lead to stabilized bed disturbances that initiate morphodynamic pattern coarsening. This study presents a kinetic interpretation of this hypothesis in terms of parameters describing particle motion. We find that the microform/mesoform transition corresponds to a transition from rarefied to collisional transport quantified by the dimensionless ratio of particle collision frequency to particle entrainment frequency. Combined with empirical relations for bedload flux and particle travel time, theory presented herein enables prediction of bed configuration under weak bedload transport conditions.

1 Introduction

Self-organized bedforms like ripples and dunes are essential equilibrium features of fluid driven sediment transport. Bedforms are germane to problems in geomorphology, river engineering, and geology because they influence macroscopic flow and sediment transport through roughness and drag partitioning effects (Einstein, 1950; Engelund & Hansen, 1967; Smith & Mclean, 1977; Fredsoe, 1982; van Rijn, 1984; Wright & Parker, 2004; Best, 2005) and produce cross-bedded sedimentary architecture that can be used to interpret past flow conditions (Paola & Borgman, 1991; Leclair & Bridge, 2001; Mahon & McElroy, 2018; Leary & Ganti, 2020). They form under a wide range of conditions; however, planar or quasi-planar topography is thought to be stable under weak bedload transport conditions near the threshold of motion in sand and gravel (Leeder, 1980; Southard & Boguchwal, 1990; van den Berg & van Gelder, 1993; Best, 1996; Carling, 1999).

Predicting the occurrence of planar topography under weak bedload transport conditions is important from a practical standpoint because (a) grain roughness is the primary source of flow resistance (Engelund & Fredsoe, 1982), (b) sediment transport is efficient because energy is not lost to form drag (Wiberg & Smith, 1989), and (c) primary current stratification lacks recognizable cross-bedded structures (Leeder, 1980; Baas et al., 2016). Weak bedload transport conditions are common in rivers and are responsible for a significant fraction of fluvial stratigraphy due to apparently universal constraints governing the geometry of self-formed channels (Lacey, 1930; Schumm, 1960; S. Ikeda et al., 1988; Dade & Friend, 1998; Eaton et al., 2004; Parker et al., 2007; Wilkerson & Parker, 2010; Métivier et al., 2017; Dunne & Jerolmack, 2018). In general, weak bedload transport conditions prevail in sand bed rivers during low discharge conditions and in gravel bed rivers when discharge is approximately equal to the formative discharge.

Despite their geomorphic and geologic significance, the mechanisms that determine whether planar topography is stable under specific flow conditions are poorly understood. Numerous studies describe turbulent flow and sediment transport processes during the initial phase of bedform initiation (Venditti et al., 2005a; Coleman & Nikora, 2009, 2011, references therein); however, these typically focus on flow conditions above the threshold of bedform development and comparisons with stable planar topography are rare. Theoretical stability analyses predict the occurrence of planar topography when mechanisms that attenuate topographic perturbations outpace amplification at every wavelength (Engelund & Fredsoe, 1982; McLean, 1990; Charru et al., 2013), but depend on continuum models for fluid, bed, and sediment phases. This is problematic because continuum models cannot capture grain-scale effects (Furbish et al., 2017) that many authors argue are an essential component of the bedform initiation process (Bagnold, 1935; Langbein & Leopold, 1968; Costello, 1974; Coleman & Melville, 1996; Coleman & Nikora, 2009). Attempts to delineate plane-bed stability fields (i.e. continuous ranges of conditions over which planar topography is stable) empirically are hindered by overlapping observations of ripples, dunes and a suite of small-scale features like bedload sheets (Whiting et al., 1988; Best, 1996; Carling, 1999; Venditti et al., 2008), particle clusters (Best, 1996; Strom et al., 2004), and low-relief bedforms (H. Ikeda, 1983; Hubbell et al., 1987; Gomez et al., 1989; Best, 1996; Carling et al., 2005) that are several particle diameters tall and are thought to be distinct from well-developed ripples and dunes due to the absence of strong flow separation and scour at the point of reattachment (Best, 1996; Seminara et al., 1996; Carling, 1999; Carling et al., 2005).

The goal of this study is to clarify the mechanisms that control the onset of ripple and dune development from lower-stage plane bed topography under weak bedload transport conditions (Figure 1). As a starting point, we propose a revised definition of lower stage plane-bed topography that encompasses quasi-planar "microforms" like bedload sheets, particle clusters, and other bedforms with amplitudes that scale primarily with particle diameter. We argue that this definition is appropriate insofar as it is aligned with the practical considerations outlined above (related to flow, sediment transport, and stratigraphy) and reflects a transition in the physical processes that govern the relief of the bed.

To elaborate this point, consider that a precise definition of lower-stage plane bed topography must recognize that the the concept of a planar bed breaks down at the granular scale. The random motion of particles driven by turbulent fluid flow causes disturbances in bed elevation (Leeder, 1980; Gyr & Schmid, 1989; Best, 1992) such that the minimum relief of a mobile bed undergoing active sediment transport is several times the nominal particle diameter (Whiting & Dietrich, 1990; Clifford et al., 1992). These disturbances tend to organize into recognizable structures due to interactions between moving particles (i.e. "kinematic clumping", Bagnold, 1935; Langbein & Leopold, 1968; Costello, 1974; Venditti et al., 2006). This occurs because particle collisions are not purely elastic. Instead, some of the kinetic energy is converted to heat in the fluid due to viscous damping effects. As a result, the difference in velocities between the two particles is less after the collision than before the collision. This effect may explain the aggregation of mobile clusters that produce localized disturbances in bed elevation when they come to rest (Coleman & Melville, 1994, 1996; Coleman & Eling, 2000; Coleman & Nikora, 2009, 2011). Stable microforms are perhaps an inevitable outcome of this process (Shinbrot, 1997).

Organized grain-scale bed disturbances may remain stable, or they may initiate pattern coarsening through nonlinear feedbacks between flow, sediment transport and topography (henceforth, "morphodynamic coarsening"). Previous studies observed the onset of significant flow separation behind disturbances (P. B. Williams & Kemp, 1971; Leeder, 1980; Best, 1996; Gyr & Kinzelbach, 2004) and defect propagation through scour-deposition waves (Raudkivi, 1963, 1966; Southard & Dingler, 1971; Costello & Southard, 1981; Gyr & Schmid, 1989; Best, 1992; Venditti et al., 2005a) when bed disturbances exceed a critical height of 2-4 particle diameters (P. B. Williams & Kemp, 1971; Leeder, 1980; Costello & Southard, 1981; Coleman & Nikora, 2009, 2011). We suggest that this threshold defines a transition in process regime that suitably differentiates morphodynamically-scaled "mesoforms" (ripples and dunes, *contra* Carling, 1999) from microforms that scale primarily with particle diameter. Below this threshold, the bed configuration may be treated as quasi-planar for most practical purposes because (a) mobile bed roughness models already include the effect of microforms (Whiting & Dietrich, 1990; Clifford et al., 1992), (b) flow separation is poorly developed such that drag partitioning effects can be ignored for the purposes of predicting sediment load, and (c) preserved cross-bedding structures have a maximum thickness of several particle diameters and are likely to be indistinguishable from planar laminations in stratigraphy.

We hypothesize that the collision-aggregation behavior described above plays a critical role in determining whether microforms achieve sufficient relief to initiate morphodynamic coarsening. Similar ideas have been promoted by numerous authors throughout the history of bedform research (Bagnold, 1935; Langbein & Leopold, 1968; Costello, 1974). Most recently, a series of papers by S. E. Coleman and others (Coleman & Melville, 1994, 1996; Coleman & Eling, 2000; Coleman & Nikora, 2009, 2011) argued that bedform initiation occurs when interactions between clusters of mobile particles cause a bed disturbance that interrupts the bedload layer. Here, we present a kinematic interpretation of this hypothesis in terms of parameters describing particle motion.

Topographic evolution occurs through the entrainment and disentrainment of individual sediment particles. Thus, we suggest that the morphodynamic importance of particle collisions may be evaluated by comparing the particle collision frequency Z_g ($\mathrm{L}^{-2}\mathrm{T}^{-1}$) (particle collision events per second per unit bed area) with the particle entrainment frequency E_g ($\mathrm{L}^{-2}\mathrm{T}^{-1}$) (particle entrainment events per second per unit bed area). The ratio $\theta = Z_g/E_g$ (henceforth, the "collision number"), characterizes the potential for particle collisions to influence topographic change and may be interpreted as the average number of collisions from entrainment to disentrainment. When $\theta <1$, collisions are rare and transport is dominated by isolated motions of individual particles. When $\theta > 1$, the average particle hop involves at least one collision, promoting the formation of mobile clusters of particles. We hypothesize that the collision behavior parameterized by θ exerts a critical control on plane-bed stability under weak bedload transport conditions. Specifically, we hypothesize that there is a threshold value $\theta \approx 1$ that separates transport conditions where planar topography is stable from transport conditions where planar topography is unstable.

In order to test this hypothesis, we quantify θ near the threshold of bedform initiation using two approaches. First, we estimate θ from experimental observations of tracer particle motion over stable and unstable planar topography using simple kinetic arguments (Kauzmann, 2012). Results of this test reveal that the transition from stable to unstable planar topography corresponds to a large increase in θ from $\theta < 1$ to $\theta > 1$ despite only a small increase in shear velocity. Second, we incorporate existing transport formulae to predict θ as a function of hydraulic and sedimentary boundary conditions. Comparison with data reported by Guy et al. (1966) and Carling (1999) indicates that the predicted threshold mirrors the transition from lower-stage plan bed topography to bedforms over a wide range of conditions. Overall, our results support the notion that particle collisions are a central feature of the bedform initiation process.

2 Theory of Particle Collisions

Here, we derive an expression for θ using a simplified, probabilistic model for bedload particle motion under statistically steady, uniform macroscopic transport conditions (Furbish, Haff, et al., 2012). This expression is central to the present research, serving two purposes. First, it enables estimation of θ using variables that can be extracted from experimental measurements of tracer particle motion discussed in Section 3. Second, the expression for θ is combined with existing empirical transport formulae to estimate θ as a function of the macroscopic state variables that govern particle motion (Section 4). This enables a direct comparson with observations of lower-stage plane bed topography and bedforms that inform classic empirical stability diagrams (Southard & Boguchwal, 1990; van den Berg & van Gelder, 1993; Carling, 1999).

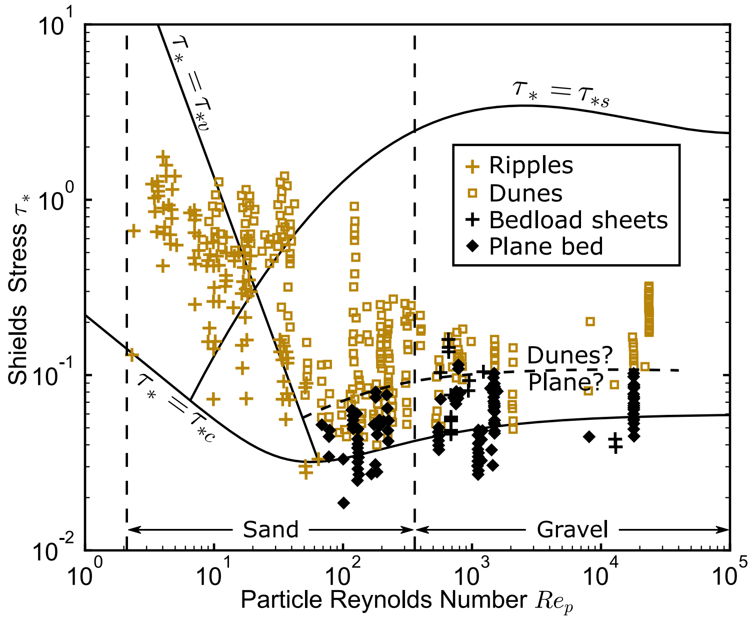

Figure 1. Shields-Parker river sedimentation diagram with empirical Plane-bed/dune threshold (dashed line) adapted from García (2008). The observations of bed configuration reported by Carling (1999) are plotted for comparison. Here, τ_{*v} is the viscous threshold Shields stress (García (2008), Equation 2-78), τ_{*s} is the suspension threshold Shields stress (Equation 2-75), and τ_{*c} is the critical Shields stress for sediment motion (Equation 2-59a). Observations of ripples and dunes below the plane/dune transition may be low-amplitude features that are distinct from well-developed ripples and dunes following Best (1996), Seminara et al. (1996), and Carling et al. (2005).

We emphasize that it is necessary to model θ from measurements of tracer particle motion rather than estimate it directly by counting collisions for two reasons. First, the term "collisions" refers broadly to interactions between particles that lead to the aggregation of mobile clusters. The details of this process are not well-understood, however it is clear that particles may exchange momentum through hydrodynamic effects even if their surfaces do not come into direct contact (Schmeeckle et al., 2001; Marshall, 2011). As a result, it is challenging to identify collisions on the basis of particle position. Second, even if collisions could be identified unambiguously, collision events are only observable if they involve two tracer particles. Because tracer particles necessarily comprise a small fraction of the bed material, observable collisions are exceedingly rare. This leads to prohibitively large uncertainty in resulting estimates of collision frequency. To illustrate this point, we note that the expected number of observable collisions in one of the experiments described below is less than 1. We did not attempt to count collisions for these reasons.

Our approach is based on the assumption that inter-particle collisions may be predicted through analogy to kinetic gas theory in two dimensions (Kauzmann, 2012). This represents the simplest possible model that captures the essential collision dynamics in a field of identical particles with randomized positions and velocities. As such, it leads to a well-defined average collision frequency that may be expressed in terms of a small number of parameters. This expression is exact when all of the underlying assumptions are valid, however it remains useful as a first-order characterization of the system when they are not. A similar approach was adopted by Bialik (2011) to predict collisions among saltating particles. Here, we summarize the derivation of this expression and discuss the extent to which it is appropriate for weak bedload transport conditions.

Throughout this study (including above), we focus primarily on count-based descriptions of particle motion like the entrainment frequency E_g ($\mathrm{L}^{-2}\mathrm{T}^{-1}$) opposed to volumetric quantities like the entrainment rate E (LT^{-1}). Count-based (granular) quantities are denoted by the subscript g, and are related to volumetric quantities by the particle volume $V_p = \pi D^3/6$, where D (L) is the nominal particle diameter. For example, $E = V_p E_g$.

Consider the circular projection of a spherical particle with diameter D moving in the two dimensional plane with constant velocity $\mathbf{u}$ (LT^{-1}) through a field of identical stationary particles. The particle of interest experiences a collision if its center passes within a distance D of another particle. Note that $\mathbf{u}$ is a vector quantity with components u and v. The magnitude of $\mathbf{u}$ (the particle "speed") is given by $|\mathbf{u}| = \sqrt{u^2 + v^2}$, where vertical lines denote vector magnitude. Over the finite time interval Δt, the number of collisions experienced by the particle of interest is equal to the number of particles contained within a rectangle with width $2D$ and length $|\mathbf{u}|\Delta t$. If the positions of the stationary particles are independent (that is, the number of particles in finite area is independent of the position of any individual particle) and there is an average of γ_g (L^{-2}) particles per unit bed area (henceforth, the "granular activity"), the particle will experience $2D\gamma_g|\mathbf{u}|\Delta t$ collisions as $\Delta t \to \infty$. It follows that the average collision frequency for the particle of interest z_g (T^{-1}) is given by

$$z_g = 2D\gamma_g|\mathbf{u}|. \tag{1}$$

Next, the effect of randomized particle motion is incorporated by considering the probability distribution of particle velocity, $f_{\mathbf{u}}(\mathbf{u}) = f_{u,v}(u, v)$ (Kauzmann, 2012). If the particle of interest is moving with velocity $\mathbf{u}_1$ and a second particle is moving with velocity $\mathbf{u}_2$, then the relative velocity of the second particle from the perspective of the particle of interest is $\mathbf{u}_2 - \mathbf{u}_1$. Assuming the positions and velocities of all particles are independent, the average collision frequency for a single particle with unknown velocity is scaled by the mean relative speed $\langle|\tilde{\mathbf{u}}|\rangle = \langle|\mathbf{u}_2 - \mathbf{u}_1|\rangle$, where angle brackets denote an average over all particles, as

$$z_g = 2D\gamma_g \langle |\tilde{\mathbf{u}}| \rangle. \tag{2}$$

Because particle velocities are assumed to be independent, the joint probability density function of velocity for any pair of particles is $f_{\mathbf{u}_1,\mathbf{u}_2}(\mathbf{u}_1, \mathbf{u}_2) = f_{\mathbf{u}}(\mathbf{u}_1) f_{\mathbf{u}}(\mathbf{u}_2)$ and the mean relative velocity for all pairs of particles is given by

$$\langle |\tilde{\mathbf{u}}| \rangle = \int \int |\mathbf{u}_2 - \mathbf{u}_1| f_{\mathbf{u}}(\mathbf{u}_1) f_{\mathbf{u}}(\mathbf{u}_2) d\mathbf{u}_1 d\mathbf{u}_2. \tag{3}$$

In a non-advecting ideal gas, the probability density function of particle velocity follows an isotropic joint normal distribution with a mean of zero and an average speed $\langle |\mathbf{u}| \rangle$. In this case, particle speed follows a Maxwell-Boltzmann distribution and equation (3) leads to $\langle |\tilde{\mathbf{u}}| \rangle = \sqrt{2} \langle |\mathbf{u}| \rangle$. Thus, the randomized motion of particles increases the collision frequency for a single particle compared to that which would be expected if other particles were stationary.

The collision frequency per unit bed area Z_g is computed from the collision frequency for a single particle by assuming there are γ_g identical particles per unit bed area, each experiencing collisions with frequency z_g. This leads to

$$Z_g = \gamma_g z_g = 2D\gamma_g^2 \langle |\tilde{\mathbf{u}}| \rangle, \tag{4}$$

Note that each collision event is counted twice (once for each particle involved in the collision) so that $\theta = Z_g/E_g$ represents the average number of collisions that a particle experiences in transit from entrainment to disentrainment.

From (4), The collision number θ may be estimated from parametric descriptions of particle motion as:

$$\theta = \frac{2D\gamma_g^2 \langle |\tilde{\mathbf{u}}| \rangle}{E_g} \tag{5}$$

An alternative formulation can be obtained under steady, uniform macroscopic flow conditions through the following equivalence:

$$E_g = \frac{\gamma_g}{T_p}, \tag{6}$$

where T_p is the average particle travel time. This expression can be obtained from the equivalent volumetric statement (Furbish, Haff, et al., 2012, Equation E5) by dividing both sides by the particle volume V_p (L^3). From (6), θ can be rewritten as

$$\theta = 2D\gamma_g \langle |\tilde{\mathbf{u}}| \rangle T_p. \tag{7}$$

A schematic interpretation of this expression is presented in Figure 2. Here, we note that $1/\theta$ is like a Knudsen number comparing the characteristic relative transport distance $L_c = \langle |\tilde{\mathbf{u}}| \rangle T_p$ with the mean free path $\lambda = [2D\gamma_g]^{-1}$ (Furbish, 1997; Furbish et al., 2017; Rapp, 2017), providing an alternative interpretation of our hypothesis. The Knudsen number quantifies whether the continuum hypothesis breaks down at a lengthscale of interest (L_c), and has important implications for the behavior of a fluid. As an example, collision shockwaves (i.e. sound) rapidly attenuate when their wavelength is smaller than the mean free path (Kahn & Mintzer, 1965; Kahn, 1966); θ therefore quantifies whether shockwaves can be propagated among bedload particles with finite transport distances. Flow is said to be “rarefied” at lengthscales below λ (Furbish et al., 2017); thus, we refer to $\theta < 1$ as the “rarefied” transport regime and $\theta > 1$ as the “collisional” transport regime.

We recognize that (5) and (7) depend on assumptions that are not strictly valid for bedload transport. For example, particle motion is driven by turbulent fluid flow such

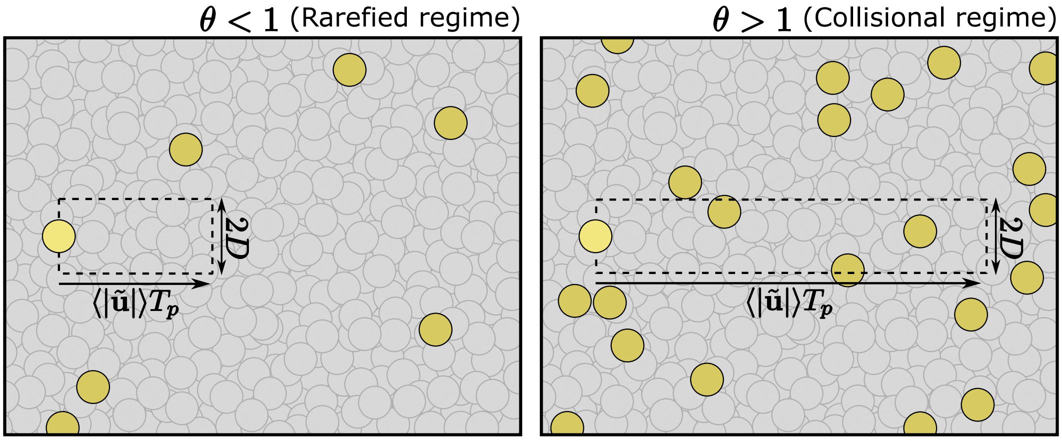

Figure 2. Schematic illustrating rarefied ($\theta < 1$) and collisional ($\theta > 1$) transport conditions. Mobile particles are shown in yellow, and immobile particles are shown in grey. A typical particle (light yellow) sweeps out a rectangle with area $2D \times \langle|\tilde{\mathbf{u}}|\rangle T_p$ during its transit from entrainment to disentrainment. The collision number θ may be interpreted as the average number of particles contained within this rectangle.

that particle velocities are not completely independent. For particle motions that are only influenced by the flow, this phenomenon leads to a correction term that modifies the mean relative velocity of particles as a function of the Stokes number (J. J. E. Williams & Crane, 1983; Sommerfeld, 2001). However, bedload transport is characterized by intermittent motions of particles that frequently interact and exchange with an immobile bed. Mobile particles may collide with immobile grains on the bed surface, decoupling their velocities from the flow in a manner that is not accounted for by Stokes-dependent correlation terms. This effect is responsible for fluctuations in particle velocity in laminar flows (Seizilles et al., 2014; Abramian et al., 2019) and is likely the dominant effect for weak bedload transport in turbulent flows because the time between particle/bed collisions is expected to be much smaller than the timescale of fluctuations in flow velocity. We assume Stokes-dependent correlations are negligible such that the mean relative velocity appropriately quantifies the collision frequency.

Following previous authors (Seizilles et al., 2014; Abramian et al., 2019), we expect that that transport may be viewed as a superposition of independent trajectories in the rarefied regime. In other words, kinetic theory provides an accurate estimate of the collision frequency when particle collisions are rare ($\theta < 1$). Although the true collision frequency may deviate from the predicted value for $\theta > 1$, we argue that our approach is sufficient (1) to delineate rarefied transport from collisional transport using observations of tracer particle motion and (2) to predict the occurrence of rarefied and collisional regimes in sand- and gravel-bedded rivers.

3 Experimental Observations of Particle Motion

3.1 Description of Experiments

Two laboratory flume experiments were conducted in order to test the hypothesis presented above. Our primary objective was to estimate θ under two conditions characterized by (a) stable and (b) unstable planar topography. Experiments were conducted in a 1.19 m wide, 14 m long flume capable of recirculating sediment and water. Flow conditions in the flume could be adjusted by varying (a) the water discharge, (b) the flume slope, and (c) the flow depth at the downstream end. We chose to vary flow conditions by changing the water discharge while holding the outlet flow depth (12 cm) and flume slope (0.001) constant. This allowed for variation in the bed stress while maintaining a constant relative submergence (the ratio of flow depth to grain size). The flow depth in the test reach was measured with a ruler and was 11 cm for both experimental conditions. Although this necessarily invokes backwater hydrodynamics, the flow may be treated as quasi-normal because the backwater length $L_{BW} = H/S$ (where H is the flow depth and S is the water surface slope) was much longer than the length of the test reach. The backwater length characterizes the spatial scale over which flow conditions vary due to backwater effects, and was approximately $L_{BW} = O(100)$ m. For comparison, the test reach was approximately 2 m; we therefore assume deviations from steady, uniform flow are negligible across the test reach.

The bed material was composed of polystyrene particles with a geometric mean diameter of 2.1 mm and a density of 1.055 g/cm^3. The base-2 logarithmic standard deviation of the grain size distribution was 0.32 (68% of the bed material had a diameter within a factor of $2^{0.32} = 1.24$ of the geometric mean), which is narrower than most naturally-sorted sediments. The dimensionless particle Reynolds number ($Re_p = \sqrt{gRD^3}/\nu$, where R is the submerged specific gravity of the sediment, ν is the kinematic viscosity of the fluid, and g is gravitational acceleration) was approximately 70.7, which is equivalent to quartz sand ($R = 1.65$) with diameter $D = 0.68$ mm. This material covered the bed of the flume in a layer that was approximately 15 cm thick. The critical Shields stress for sediment motion estimated from the the formula of Brownlie (1981) was $\tau_{*c} = 0.032$.

In order to achieve flow conditions straddling the the threshold of bedform development, we initially allowed topography to equilibrate to a discharge known to produce bedload dominated bedforms (35 L/s). Then, we incrementally reduced the discharge by 5 L/s until planar topography was observed. The bed configuration was allowed to adjust over a period of 24 hours after each reduction in discharge. Using this procedure, we established that plane-bed topography was stable at a water discharge of 20 L/s while bedforms were stable at a water discharge of 25 L/s. Measurements of flow velocity, bed topography, and particle motion were collected over equilibrium lower-stage plane topography as described in more detail below. Discharge was then increased to 25 L/s and identical measurements were immediately made over unstable plane-bed topography. Finally, the bed configuration was allowed to equilibrate to the increased water discharge for roughly 24 hours to verify the presumed instability.

Flow velocity and bed elevation profiles were measured using a Nortek Vectrino Profiler acoustic Doppler velocimeter (ADV). The ensemble average flow velocity profile was computed at a resolution of 2 mm using a sampling procedure that produced a total of 105 s of velocity data at each elevation measured at a frequency of 30 Hz. The sampling procedure was designed to allow estimation of the Reynolds-averaged flow velocity at each elevation in the flow using samples of the three-dimensional velocity vector obtained over a finite spatial and temporal extent. This procedure is justified because the flow conditions are approximately steady and uniform, and the sample is much larger than the spatiotemporal scales of flow velocity correlation. To obtain a representative sample of flow velocity, the ADV was mounted to a moving cart and moved upstream and then back downstream along a 2 m longitudinal transect in the center of the flume at a speed of 3.8 cm/s. Because flow velocity is measured relative to the profiler head, the longitudinal velocity of the cart was subtracted from the measured velocity vector. The profiler was capable of measuring flow velocity over a range of 1.6 cm at any instant; full velocity profiles from the bed surface to within 3 cm of the water surface (approximately 8 cm from the bed) were constructed by repeating this procedure at 5 different vertical positions. This was accomplished using a fully automated routine wherein the position and velocity of the instrument was recorded concurrently with flow velocity data. Measured velocity profiles did not deviate significantly between upstream and downstream segments of the reach, verifying our assumption that gradually varied flow effects can be ignored.

Shear velocity was estimated using a linear least-squares fit to the log-transformed velocity profile (Bagherimiyab & Lemmin, 2013). For the 25 L/s (unstable plane bed) condition, the measured velocity profile followed the logarithmic law of the wall from 1 cm above the bed to the top of the profile (8 cm above the bed). Although the law of the wall is only strictly valid in the lower portion of the flow, the velocity in the interior of the flow is not expected to deviate significantly from a logarithmic profile under quasi-steady, uniform flow conditions (Townsend, 1976; Wilcock, 1996; Winterwerp & van Kesteren, 2004). We find that the estimated shear velocity is not sensitive to range of depths considered as long as the portion below 1 cm is excluded. Shear velocity estimated using this procedure was 0.94 cm/s, and the dimensionless Shields stress $\tau_* = u_*^2/gRD$ was 0.077.

For the 20 L/s (stable plane bed) condition, measured flow velocities follow the logarithmic law of the wall from 3 cm above the bed to 8 cm above the bed. Below 3 cm, the mean velocity follows an irregular profile. We attribute this profile to a data artifact that was not recognized at the time of data collection. Although the velocity data are questionable, shear velocity estimated using velocity measurements obtained over the logarithmic region of the flow was 0.77 cm/s. The Shields stress estimated using this procedure was $\tau_* = 0.52$. We are confident that this estimate is reasonable because (a) the Shields stress must be less than the 25 L/s condition due to the reduced discharge, (b) the Shields stress must be greater than the critical Shields stress for sediment motion, and (c) a similar estimate is obtained from the measured bedload flux. For additional discussion of the measured flux and associated estimate of shear velocity, see Section 3.4.

Bed elevation profiles measured concurrently with velocity data were used to quantify variability in bed elevation characteristic of qualitatively planar topography in our experiments. Small surface undulations with slopes well below the angle of repose (maximum 3 degrees) and heights of roughly $3D$ are evident under stable and unstable plane-bed conditions. After the bed was allowed to equilibrate to the 25 L/s water discharge condition, we observed well-developed “3D” dunes (*sensu* Venditti et al., 2005b) with measured lee slopes at the angle of repose (maximum 35 degrees). Two bedform crests were visually identified in six repeat longitudinal profiles collected at 105 second intervals. These profiles covered 2 m of the bed at a spatial resolution of 1 cm. Bedform length computed as the average distance between the highest point of the crests in all six scans was 64 cm. The bedform height computed as the average height from the highest point of each crest to the lowest point before the next crest was 2.9 cm. The migration velocity estimated by averaging the displacement of the individual crests between scans was 1.4 cm/minute. Although more sophisticated methods exist for quantifying the characteristic scales of bedform topography, this approach is sufficient for our purposes.

3.2 Particle Tracking

Parameters describing the kinematic properties of particle motion were extracted from manually-digitized tracer particle paths. To this end, a small fraction of the bed material was removed from the flume and coated with a thin layer of fluorescent spray paint. These particles were then added back to the flume and allowed to mix with the bed material under a range of flow conditions prior to these experiments. Illuminating the bed with a blacklight increases the contrast of tracer particles relative to other particles so that individual particles can be confidently tracked over long durations. This procedure also significantly reduces the number of particles that need to be tracked in order to obtain a representative sample of particle behavior (Naqshband et al., 2017; Ashley, Mahon, et al., 2020).

Videos of tracer particle motion were recorded using a downward facing digital camera attached to a fixed boom 2.05 m above the water surface. Because the flow velocities needed to mobilize the polystyrene particles were low relative to quartz sand, particles could be tracked through the water surface with a high degree of precision. Image rectification (which corrects for image distortion due to slight misalignment of the camera), and registration (which establishes a coordinate system in the correct units allowing for conversion from pixel position to bed position) were performed with known reference points in the flume using OpenCV (Bradski, 2000) in Python. Manual digitization of particle motions was performed using TrackMate (Tinevez et al., 2017), an open source particle tracking package for ImageJ (Schindelin et al., 2012). In order to minimize sampling bias, all tracer particle motions that occurred within the sampling window during the specified time interval were tracked. Two ten second videos comprising a total of twenty seconds of observations from each experiment were used for this study. After registration, rectification, and trimming, both videos covered a streamwise distance of 210 cm and a cross-stream distance of 99 cm. Particle behavior is sensitive to inevitable variations in shear stress that occur in the cross-stream direction (Abramian et al., 2019). For this reason, analyses reported here were performed using particle motions that occurred within a 30 cm wide, 2 m long control volume in the center of the flume corresponding to the location where shear stress was estimated from flow velocity measurements. We note that the initial phase of bedform growth began in this region and then propagated laterally to the edges of the flume. Tracked particle paths are plotted in Figure 3.

Videos were recorded at a framerate of 30 Hz and a resolution of roughly 9.4 pixels per cm at the bed surface. Videos were downsampled to a resolution of 4.7 pixels per cm so that raster data could be stored without compression in computer memory. After rectification and registration, the length of each pixel was 2.1 mm (approximately the nominal particle diameter). Fluorescent tracer particles create a halo that illuminates adjacent pixels, and differences in pixel brightness enable robust estimation of the particle centroid location at sub-pixel resolution (Leary & Schmeeckle, 2017).

Particle tracking software records particle location with an arbitrary degree of precision depending on image magnification; thus, particles which are qualitatively identified as immobile may possess nonzero measured velocities. Following previous studies (e.g., Lajeunesse et al., 2010; Liu et al., 2019; Ashley, Mahon, et al., 2020), we employed a velocity threshold criteria to distinguish mobile and immobile particles. Velocity criteria are useful because they provide a reproducible solution to this problem, and because sensitivity analysis can easily be conducted by varying the value of the velocity threshold (Section 5.1). For additional discussion of velocity criteria, see (Ashley, Mahon, et al., 2020) and references therein. Recognizing that the motion state of certain particles is unclear, we inspected motions identified using a range of velocity thresholds and found that visual identification of particle motion corresponded to values of the velocity threshold ranging from $u_c = 0.005$ m/s to $u_c = 0.01$ m/s. Below 0.005 m/s, particles which remain in the same location for significant durations are identified as mobile, and above 0.01 m/s, particles which are clearly in motion in the bedload phase are identified as immobile. The exact values of certain computed quantities are sensitive to the specific choice of velocity threshold within this range, however the primary findings of this work are not. Detailed sensitivity analysis was performed using velocity thresholds ranging from 0.0001 m/s to 0.1 m/s and is discussed in detail in Section 5.1. Reported results were obtained using a velocity threshold of 0.007 m/s, which is approximately the geometric midpoint of the optimum range (0.005 m/s to 0.01 m/s).

In order to compute certain bulk statistics of sediment transport from tracer particle statistics, it was necessary to estimate the tracer fraction in the flume. This was accomplished by collecting a sample of material within a few centimeters of the bed surface from three locations spread across the bed after the experimental campaign was com-

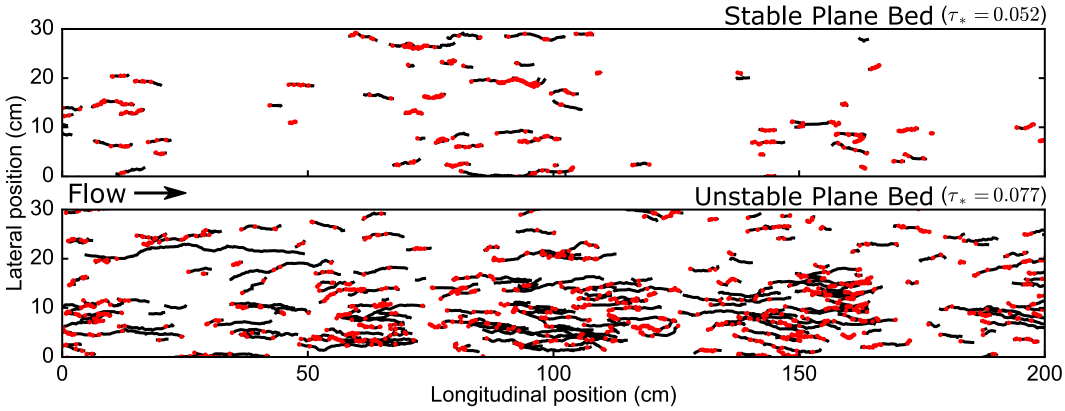

Figure 3. Tracer particle paths (black lines) and entrainment event locations (red dots) for stable and unstable plane bed experiments. Data are from the same total duration for both experiments (20 s) such that apparent differences in the densities of black lines and red dots are representative of the relative sediment loads and entrainment frequencies.

plete. Tracer particles are expected to be evenly distributed in this region due to the migration of bedforms. The total mass of the sample was 760 g. Tracer particles were separated by hand under a blacklight and then weighed. The total mass of tracer particles in the sample was 1.49 g. Thus, we estimate the tracer fraction to be 0.00196.

3.3 Methods for Computing Particle Motion Statistics From Digitized Particle Paths

3.3.1 Particle Position and Velocity

The kinematic statistics of particle motion needed to estimate θ using equation (5) were computed from digitized particle paths following Ballio et al. (2018). We consider digitized particle motions within a control volume extending from the flume bottom to the water surface projected onto a 2 dimensional plane A (Figure 3). Each particle motion is defined by a sequence of discrete measurements of particle position on the domain of longitudinal position x and lateral position y. The position of the i^{th} of m tracked particles in the j^{th} of n frames is expressed by the vector $\mathbf{x}_{i,j}$ with longitudinal and lateral components $x_{i,j}$ and $y_{i,j}$.

Particle velocities are computed by comparing subsequent positions of a particle. Measured velocities therefore represent temporal averages between the two measurements of particle position; however, the time between frames δt is sufficiently small that it may be viewed as an instantaneous velocity for our purposes. This assumption may be evaluated by comparing δt to the timescales characterizing fluctuations in particle velocity. Furbish, Ball, and Schmeeckle (2012) argue that the velocity signal must possess a fundamental harmonic with period $T = 2T_p$, implying that in the most basic sense, the mean particle travel time sets the primary scale of fluctuations in particle velocity. We estimate $T_p >> \delta t$ for both experiments.

The velocity vector $\mathbf{u}_{i,j}$ with longitudinal and lateral components $u_{i,j}$ and $v_{i,j}$ is computed as

$$\mathbf{u}_{i,j} = \frac{\mathbf{x}_{i,j+1} - \mathbf{x}_{i,j}}{\delta t}. \tag{8}$$

Thus, the velocity attributed to frame j represents the average velocity between frame j and frame $j+1$.

3.3.2 Mean Granular Activity γ_g

The mean granular activity is computed by counting the number of active tracer particles in the control volume in each frame and averaging. This is accomplished using an Eulerian clipping function M^A to quantify whether the i^{th} tracer particle is within the control area A in the j^{th} frame:

$$M^A_{i,j} = \begin{cases} 1, & \text{if } \mathbf{x}_{i,j} \in A \\ 0, & \text{otherwise} \end{cases}. \tag{9}$$

Additionally, a velocity threshold u_c is used to define the state of motion of a particle quantified by the clipping function M^m:

$$M^m_{i,j} = \begin{cases} 1, & \text{if } |\mathbf{u}_{i,j}| \geq u_c \\ 0, & \text{otherwise} \end{cases} \tag{10}$$

Thus, the number of mobile tracer particles in the control volume in frame j is given by:

$$N^{m,A}_j = \sum_{i=1}^{m} M^m_{i,j} M^A_{i,j}. \tag{11}$$

Tracer particle positions recorded in n frames lead to $n-1$ measurements of velocity, and the average number of moving tracer particles within the control volume over all frames with valid velocity measurements is given by:

$$\langle N^{m,A} \rangle = \frac{1}{n-1} \sum_{j=1}^{n-1} N^{m,A}_j. \tag{12}$$

Here, angle brackets denote sample averages which provide unbiased estimates of the ensemble assuming ergodicity.

The granular activity is estimated by dividing $\langle N^{m,A} \rangle$ by the tracer particle fraction ψ and the control volume area:

$$\gamma_g = \frac{\langle N^{m,A} \rangle}{\psi A}. \tag{13}$$

Note that γ_g is an an estimate of a mean, but angle brackets are dropped to simplify notation in Section 2.

3.3.3 Mean Speed $\langle|\mathbf{u}|\rangle$ and Relative Speed $\langle|\tilde{\mathbf{u}}|\rangle$

The mean speed of moving tracer particles in the control volume is estimated as

$$\langle \mathbf{u}^{m,A} \rangle = \frac{1}{(n-1)\langle N^{m,a} \rangle} \sum_{i=1}^{m} \sum_{j=1}^{n} \mathbf{u}_{i,j} M^m_{i,j} M^A_{i,j} \tag{14}$$

where $(n-1)\langle N^{m,a} \rangle$ is the total number of measurements of tracer particle speed that exceed the threshold speed. The mean longitudinal particle velocity $\langle u \rangle$ can be estimated by substituting the longitudinal component of $\mathbf{u}$ for $\mathbf{u}_{i,j}$ in (14). Once the granular activity γ_g and $\langle u \rangle$ are known, The ensemble average granular particle flux characteristic of macroscopic flow conditions q_{sg} ($\mathrm{L}^{-1}\mathrm{T}^{-1}$) may be estimated as $q_{sg} = \gamma_g \langle u \rangle$.

The mean relative speed of tracer particles is estimated by taking the average of the difference between all measured particle speeds in the control volume, i.e.:

$$\langle|\tilde{\mathbf{u}}^{m,A}|\rangle = \frac{1}{[(n-1)\langle N^{m,a} \rangle]^2} \sum_{i=1}^{m} \sum_{j=1}^{n} \sum_{k=1}^{m} \sum_{l=1}^{n} |\mathbf{u}_{i,j} - \mathbf{u}_{k,l}| M^m_{i,j} M^A_{i,j} M^m_{k,l} M^A_{k,l} \tag{15}$$

3.3.4 Granular Entrainment Frequency E_g

The final relevant quantity that must be estimated to compute θ with equation (7) is the entrainment frequency E_g. Entrainment and disentrainment events are defined as transitions between the mobile and immobile states and are quantified by differentiating M^m with respect to time (Ballio et al., 2018). Following this approach, we define an entrainment function M^E as

$$M^E_{i,j} = M^m_{i,j} - M^m_{i,j-1}. \tag{16}$$

This function may take on values of 1, 0, or -1, signifying an entrainment event, no event, or a disentrainment event. Assuming the spatially-averaged time rate of change of bed elevation is zero within and around the control volume, the entrainment frequency E_g and the disentrainment frequency D_g must be equal. Consequently, the spatially averaged entrainment and disentrainment frequencies can be estimated from the absolute value of M^E as

$$E_g = D_g = \frac{1}{(n-2)\delta t} \sum_{i=1}^{m} \sum_{j=2}^{n-1} \frac{1}{2} |M^E_{i,j}| M^A_{i,j}. \tag{17}$$

Here, $(n-2)\delta t$ is the total time over which it is possible to detect entrainment events occurring in n frames. The mean travel time T_p may then be estimated from E_g and γ_g using (6). This estimate of T_p is not biased by particles entering or leaving the control volume.

3.4 Experimental Results

For the stable plane bed condition, the experimental procedure described above yielded a total of 3168 measurements of particle speed in excess of the threshold speed in the control volume belonging to 70 unique particles (Figure 3). The entrainment function (equation 16) was used to identify a total of 798 tracer particle exchanges with the bed (entrainment and disentrainment events). The ensemble average tracer particle flux was 0.22 particles per second per meter width. This leads to a total granular flux $q_{sg} = 114$ particles per second per meter width and a dimensionless bedload flux $q_* = q_g V_p / \sqrt{RgD^3}$ of 0.0078. Solving the Wong and Parker (2006) bedload equation for shear velocity using the critical Shields stress predicted from Brownlie (1981) leads to $u_* = 0.74$ cm/s compared with 0.77 cm/s estimated using acoustics.

For the unstable plane bed condition, experiments produced 16075 measurements of mobile particles in the control volume belonging to 238 unique particles (Figure 3). The entrainment function identified 2461 exchanges with the bed. The ensemble average tracer particle flux was 1.4 particles per second per meter width leading to a total granular flux of $q_{sg} = 688$ particles per second per meter width and a dimensionless bedload number of $q_* = 0.047$. The shear velocity estimated from q_* was $u_* = 0.98$ cm/s compared with 0.94 cm/s estimated using acoustics.

Experimental results are reported in Table 1. Notably, the collision number varies by almost a factor of 10 between the two experiments from 0.15 to 1.35. In terms of the Knudsen number interpretation of θ, the observed difference reflects both an increase in the characteristic transport length $\langle|\tilde{\mathbf{u}}|\rangle T_p$ and a decrease in the mean free path λ.

4 Comparison with Empirical Stability Diagrams

In Section 3, we estimated θ from observations of tracer particle motion to quantify collision behavior for two experimental conditions straddling the threshold of bedform development. Here, we investigate collisional behavior a wide range of conditions by combining existing theoretical and empirical relations to obtain an expression for θ

Table 1. Summary of Experiments

	Stable plane bed	Unstable plane bed
Boundary Conditions		
Geometric mean particle diameter D	2.1 mm	2.1 mm
Sediment density ρ_s	1.055 g/cm^3	1.055 g/cm^3
Particle Reynolds Number Re_p	70.7	70.7
Unit water discharge q_w	0.016 m^2/s	0.021 m^2/s
Flow depth in test area h	0.11 m	0.11 m
ADV Shear velocity u_*	0.0077 m/s	0.0094 m/s
Shields stress τ_*	0.052	0.077
Results		
Granular activity γ_g	4500 m^{-2}	23,800 m^{-2}
Mean relative speed $\langle\vert\tilde{\mathbf{u}}\vert\rangle$	2.9 cm/s	3.3 cm/s
Mean longitudinal velocity $\langle u\rangle$	2.5 cm/s	3.0 cm/s
Entrainment frequency E_g	17000 m^{-2}s^{-1}	52400 m^{-2}s^{-1}
Mean travel time T_p	0.26 s	0.43 s
Granular sediment flux q_{sg}	114 m^{-1}s^{-1}	688 m^{-1}s^{-1}
Volumetric sediment flux q_s	5.53 $\times 10^{-7}$ m^2/s	3.34 $\times 10^{-6}$ m^2/s
Collision frequency Z_g	2550 m^{-2}s^{-1}	70700 m^{-2}s^{-1}
Einstein bedload number q_*	0.008	0.047
Mean free path λ	5.3 cm	1.0 cm
Characteristic transport length L_c	0.8 cm	1.3 cm
Collision number θ	**0.15**	**1.35**

in terms of the macroscopic state variables that govern particle motion. Specifically, we derive an expression of the form

$$\theta = f(\tau_*, Re_p). \tag{18}$$

such that the hypothesized threshold of bedform initiation can be represented as $f(\tau_*, Re_p) = 1$. This expression is compared with observations of planar topography and bedforms to evaluate whether our hypothesis can explain trends in empirical data (van den Berg & van Gelder, 1993; Southard & Boguchwal, 1990; Carling, 1999; García, 2008).

The first element needed to derive (18) is a model relating the mean relative speed $\langle|\tilde{\mathbf{u}}|\rangle$ to the mean longitudinal velocity $\langle u\rangle$. This expression is necessary because the mean relative speed is an obscure quantity that is not referenced in existing literature. In contrast, the mean longitudinal velocity is an essential component of the flux and is relatively well-studied (Lajeunesse et al., 2010, references therein). These quantities may be related by assuming a joint probability distribution model for longitudinal and lateral particle velocity. Several authors have proposed functional forms for the margins of this distribution (e.g., Furbish & Schmeeckle, 2013; Fathel et al., 2015; Furbish et al., 2016; Liu et al., 2019); however, the correlation behavior and relative magnitudes of longitudinal and lateral components are not well-constrained, precluding the possibility of a purely theoretical derivation. Instead, we assume

$$\langle|\tilde{\mathbf{u}}|\rangle = \alpha\langle u\rangle, \tag{19}$$

where α is a coefficient of order unity. Neglecting lateral motions and assuming longitudinal velocities follow an exponential distribution as expected for particle motions over planar topography (Fathel et al., 2015; Ashley, Mahon, et al., 2020) leads to $\alpha = 1$. This may be interpreted as a lower bound because upstream motions and nonzero lateral velocities will increase the mean relative speed with respect to the mean longitudinal ve-

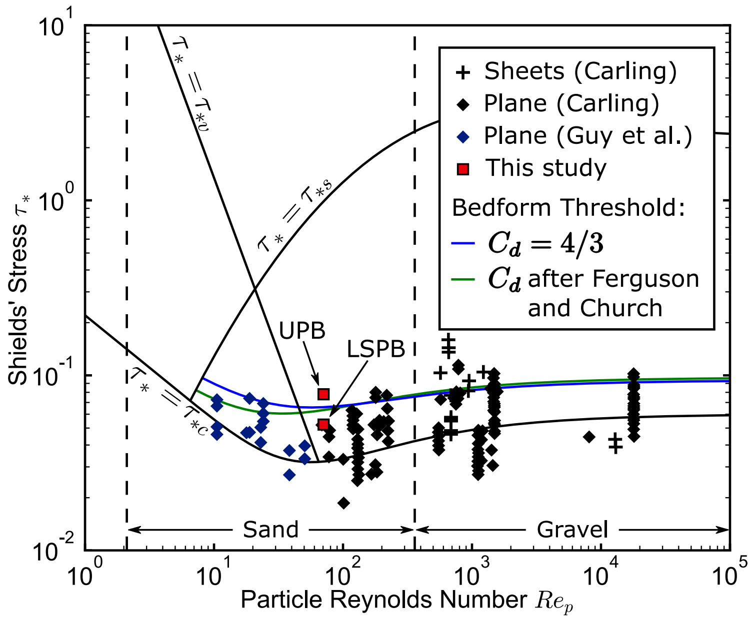

Figure 4. Shields-Parker river sedimentation diagram with theoretical plane-bed/bedform transition (Equation 25) for two particle settling models. As expected, the stable plane bed experiment (SPB) plots below the threshold while the unstable plane bed experiment (UPB) plots above the threshold. Observations of planar topography and bedload sheets reported by Carling (1999) are plotted for comparison. Also plotted are observations of planar topography reported by Guy et al. (1966) that were ignored by Southard and Boguchwal (1990) and van den Berg and van Gelder (1993) in delineating classic stability fields.

locity. We find that α computed directly from data is close to 1 despite lateral and upstream motions: $\alpha = 1.08$ for the stable plane bed condition and $\alpha = 1.13$ for the unstable plane bed condition. This indicates that upstream and lateral motions do not contribute significantly to the total collision frequency. Instead, most collisions occur primarily because fast-moving particles overtake slow-moving particles. For simplicity, we assume $\alpha = 1$, noting that other realistic values do not influence the analysis presented below.

Next, we combine (19) with the activity form of the average flux in the bedload phase q_b under steady, uniform transport conditions (Furbish, Haff, et al., 2012) given by

$$q_b = \gamma \langle u \rangle. \tag{20}$$

This leads to

$$\theta = \frac{12\alpha q_b T_p}{\pi D^2}. \tag{21}$$

Recall that the volumetric and granular activity are related by the particle volume as $\gamma = \gamma_g V_p$.

The next element needed to obtain (18) is an empirical relation for the mean particle travel time T_p. This is perhaps the most uncertain element in predicting θ, owing in part to experimental censorship and discrepancies in the strategies employed in different studies to delineate mobile and immobile particles (Hosseini-Sadabadi et al., 2019). Lajeunesse et al. (2010) reviewed previous work and concluded based on physical and dimensional arguments that the mean travel time should be predicted as

$$T_p = \beta \frac{D}{\omega_s} \left(\frac{u_* - u_{*c}}{\omega_s} \right)^{\varepsilon} \tag{22}$$

where ω_s is the particle settling velocity, u_* is the shear velocity, u_{*c} is the critical shear velocity for sediment motion, and β and ε are empirical coefficients. Based on available data, they suggest that $\beta = 10.7$ and $\varepsilon = 0$, removing the dependence on u_*. We recognize that the particle travel time may possess a weak dependence on u_* despite this result. However, this does not affect the present analysis as a nonzero value of ε does not influence the trends in θ as a function of τ_* and Re_p (we return to this point below). The settling velocity is given by $\omega_s = \sqrt{4RgD/3C_d}$, where C_d is a drag coefficient. Combining equations (21) and (22) with suggested values for α and β leads to

$$\theta = 44.2\sqrt{C_d} q_* \tag{23}$$

where $q_* = q_b/\sqrt{gRD^3}$ is the Einstein bedload number.

Finally, the empirical bedload transport equation of Wong and Parker (2006), given by

$$q_* = 3.97(\tau_* - \tau_{*c})^{3/2}, \tag{24}$$

is substituted into (23) to obtain an an expression taking the form of (18). Solving for the Shields stress τ_* corresponding to $\theta = 1$ leads to an prediction of the critical stress for bedform initiation:

$$\tau_* = \left(\frac{1}{175\sqrt{C_d}} \right)^{2/3} + \tau_{*c} \tag{25}$$

where $\tau_{*c} = f(Re_p)$ after Brownlie (1981) and $C_d = f(Re_p)$ after Ferguson and Church (2004).

The stability field for lower-stage plane bed topography implied by this expression is plotted in Figure 4. We note that neglecting viscous settling ($C_d \approx 4/3$) following Lajeunesse et al. (2010) results in almost no change in the stability field for lower-stage plane bed topography. Nonzero values of ε lead to a slightly different form for equation (25) because θ has an additional dependence on $[0.75C_d(\tau_* - \tau_{*c})]^{\varepsilon/2}$. However, this effect essentially shifts isocontours of θ up or down while preserving the qualitative trends in θ. We emphasize that this model is derived assuming that bedform initiation occurs under bedload-dominated transport conditions. This assumption is critical, both for the collision model described in Section 2, and to scale the flux in Equation (24). The stability field for lower-stage plane bed topography computed using (25) is not plotted above the threshold of significant suspension in Figure 4 for this reason.

Observational data complied by Carling (1999) are plotted in Figure 4 for comparison with theory. This figure also includes observations of planar topography reported by Guy et al. (1966) that were ignored in subsequent studies because they are within the hydraulically smooth regime. Southard and Boguchwal (1990) asserted that these conditions would have eventually produced ripples, however we suggest that the relief of stable ripples would be small leading to poorly-developed flow separation. As a result, they could be considered quasi-planar microforms by the criteria proposed above. The proposed stability field for lower-stage plane bed topography mirrors the empirical stability fields delineated using this observational data (Figure 1) but extends into the hydraulically smooth regime.

5 Discussion

Sections 3 and 4 describe two tests designed to evaluate whether interactions between moving particles are responsible for a transition in the processes governing sedimentary bed relief. Based on observations by previous authors (e.g., Coleman & Nikora, 2011), we hypothesized that plane-bed topography is stable in the rarefied transport regime corresponding to $\theta < 1$, and becomes unstable in the collisional regime above a critical value $\theta \approx 1$. Experimental observations of tracer particle motion presented in Section 3 support this hypothesis: we find that the transition from lower-stage plane bed topography to bedforms corresponds to a large increase in θ from 0.15 to 1.35 despite only a small increase in shear velocity. Theoretical extrapolation discussed in Section 4 illustrates how our hypothesis leads to a prediction of the threshold of bedform initiation that mirrors classic empirical stability diagrams. Overall, these results support the hypothesized causal link between particle collisions and bedform development.

Here, we consider the theoretical implications of this finding and argue that our results are entirely consistent with existing studies describing bedform initiation and stability. This is accomplished by reexamining the arguments used to justify our hypothesis. In Section 1, we argued that well-developed ripples and dunes are distinct from microforms like bedload sheets, particle clusters, and low-amplitude ripples and dunes due to a transition in processes governing the relief of the bed. Three mechanisms are invoked to explain this transition.

First, we suggest that microforms are an inevitable outcome of fluid driven sediment transport. This follows from the notion that quasi-random motions of particles produce grain-scale disturbances in bed elevation. The formation of grain-scale disturbances driven by turbulent fluid flow has been described by a number of authors (P. B. Williams & Kemp, 1971; Best, 1992); Whiting and Dietrich (1990) and Clifford et al. (1992) argue that the difference between fixed- and mobile- bed roughness is explained by this phenomenon. More generally, we suggest that microforms are a manifestation of inevitable self-organization of granular bed disturbances through damped particle collisions (Shinbrot, 1997).

Second, we suggest that microform amplitude scales with particle diameter and collision frequency. Coleman and Nikora (2009, 2011) argued that interactions between mobile clusters of particles increase the size of disturbances in bed elevation. This implies that there is a balance between disturbance growth and decay, where growth is related to particle collisions and decay is related to disturbance size. The process of disturbance decay may reflect a tendency for particle erosion and deposition to be inversely correlated with elevation: particles at high elevations are more exposed to turbulent flow and thus more likely to be entrained than particles at low elevations, while mobile particles are more likely to be deposited in topographic lows that are relatively sheltered. This process may be mathematically analogous to the slope effect that is commonly invoked in linear stability analyses (Charru et al., 2013). We suggest here that the stable microform amplitude H_μ is related to the collision number, for example as $H_\mu/D \propto \theta$.

Finally, we suggest that microforms are stable up to a critical amplitude, above which flow separation and scour at the point of reattachment lead to morphodynamic coarsening. Studies that describe bedform growth from artificial or natural defects typically find that small defects are suppressed rather than amplified (Southard & Dingler, 1971; Gyr & Schmid, 1989; Gyr & Kinzelbach, 2004; Venditti et al., 2005a; Coleman & Nikora, 2009). Only when defects exceed a critical height, usually reported as a constant multiple of particle diameter ranging from 2-4, do they stabilize and propagate (P. B. Williams & Kemp, 1971; Leeder, 1980; Costello & Southard, 1981; Coleman & Nikora, 2009, 2011). This transition in process regime fundamentally distinguishes quasi-planar configurations from well-developed ripples and dunes.

We note that empirical stability fields for planar topography and bedforms overlap substantially, with many observations of bedforms occurring under conditions that are predicted to produce rarefied transport. We offer several possible explanations. First, low-amplitude bedforms with poorly developed flow separation could potentially appear qualitatively similar to ripples and dunes in planform. In this case, they might be labeled as bedforms while being more appropriately classified as microforms in the context of the present research. Alternatively, the overlap may reflect uncertainty in estimates of Shields stress, which is large for low values near the threshold of motion. Finally, the observed overlap may be a genuine feature of the data. If this is true, it implies that the method for constraining the threshold of bedform initiation as a function of τ_* and Re_p is incomplete and merely provides an upper limit for plane-bed stability. In this case, the bed configuration likely depends on an additional parameter not considered here due to either (a) violations of our simplified collision model that cause true values of the collision frequency to deviate from kinetic theory, (b) physical mechanisms that influence the critical value of θ for bedform initiation. The particle Stokes number, Froude number, and relative particle submergence are not uniquely constrained by τ_* and Re_p and therefore parameterize variability that is not represented in Figure 4. It is likely that several effects are relevant; for example, θ may vary with respect to the estimate provided by (23) as a function of particle Stokes number. The maximum stable microform amplitude may be approximately 3-4 particle diameters in general, but may depend in detail on the relative submergence of particles. Simultaneously the stable microform amplitude may depend on θ and the Froude number. If these effects exist, they are obscured by uncertainty in τ_*. Nevertheless, we argue that the first-order constraint on bed configuration proposed by this study is valuable, even if it only provides an upper limit.

We emphasize that our results are compatible with mathematical analyses that examine instability arising from the coupled evolution of flow, sediment transport, and topography (e.g., Engelund & Fredsoe, 1982; McLean, 1990; Andreotti et al., 2010; Charru et al., 2013). These studies are rooted in continuum models that imply averaging over the granular descriptions of transport considered here. Our results may help explain and/or refine continuum models of bedform initiation by elucidating how they emerge from granular mechanics. To clarify this point, consider that a slope effect is often invoked to predict a finite fastest-growing wavelength near the threshold of sediment motion (Andreotti et al., 2010; Charru et al., 2013). Mathematically, the slope effect is introduced through a proportional modification of the transport capacity that is proposed based on reasonable arguments but lacks a clear physical basis. We suggest that the the collision/aggregation behavior considered here may provide provide direct justification for the slope effect in terms of granular motion, or may lead to an alternative description of bedform stability in the continuum limit.

An interesting outcome of Section 4 is that the transition from rarefied to collisional transport predicted from (25) is similar to the to the threshold of continuous transport described by other authors (e.g., González et al., 2017; Pähtz et al., 2020). This threshold is characterized by a profound reduction in transport intermittency (i.e., variability in the total momentum of particles over a finite bed area) and occurs at roughly $\tau_* = 2\tau_{*c}$. Despite arising from disparate descriptions of sediment motion, we suggest that the concepts of intermittent and rarefied transport are intuitively similar, and that their alignment ultimately reflects compatible physical reasoning and consistent scaling of transport parameters like particle activity and velocity with Shields stress.

5.1 Sensitivity of Results to the Choice of Mobility Threshold u_c

The main objective of this exercise is to determine whether small changes in u_c influence our conclusions regarding θ. While the values of θ are sensitive to u_c, we find that the the value for the unstable plane bed condition exceeds the value for the stable plane bed condition by a factor of approximately 10 across the full range of u_c values tested (Figure 5A). We also find the value for the unstable plane bed condition exceeds 1 while the value for the stable plane bed condition is less than 1 for reasonable values of u_c identified by inspecting particle motions. Above $u_c \approx 0.1$ m/s, we find $\theta < 1$ for the unstable plane bed experiment, however this result is unrealistic because clearly mobile particles are ignored. Furthermore, $\theta = \mathrm{O}(1)$ up to $u_c \approx 0.025$ for the unstable plane bed condition. For comparison, $\theta = \mathrm{O}(0.1)$ across this range for the stable plane bed condition. While results obtained using 0.01 m/s $< u_c <$ 0.025 m/s independently are equivocal, we argue that the behavior of θ as a function of u_c is expected and holistically supports the hypothesis and interpretations discussed above.

Estimates of tracer particle flux, total granular flux, and volumetric flux (which are related by the tracer fraction and nominal particle volume) are also not sensitive to u_c across the optimum range. However, computed sediment load decreases rapidly for $u_c >$ 0.02 m/s because particles that contribute significantly to the measured sediment load are ignored (Figure 5B). This observation provides a quantitative upper bound for u_c and supports the notion that θ values computed above this bound are unreasonable. In contrast, arbitrarily low values of u_c provide consistent estimates of flux. This is also expected; recall that the flux is calculated as $q_b = \gamma_g \langle u \rangle$. Including immobile particles with near-zero velocities in the calculation of sediment load increases γ_g but decreases $\langle u \rangle$ by reciprocal factors such that there is no change in estimates of q_b.

Other relevant quantities (for example, entrainment rates, activities, velocities) are sensitive to the choice of velocity threshold. Computed quantities typically vary slowly as monotonic functions of u_c up to the point where u_c is a significant fraction of the maximum measured particle speed (roughly $u_c = 0.02$ m/s in our experiments). Above this threshold, computed quantities vary rapidly with u_c as mobile particles are increasingly ignored. The average particle speed (the magnitude of the velocity vector) exemplifies this behavior (Figure 5C). Interestingly, we find that the difference between the mean computed particle speed and the threshold speed ($\langle |\mathbf{u}| \rangle - u_c$) is maximized across the optimum range of velocity values that was determined independently by inspecting particle motions. Below this range, immobile particles included in the computation of mean velocity cause a decrease in the excess particle speed; above, the threshold speed begins to approach the maximum measured particle speed. This observation potentially provides an objective approach for selecting a velocity threshold.

6 Conclusions

This study clarifies the nature of lower-stage plane bed topography and the granular mechanics of ripple and dune initiation. As a starting point, we recognize that the concept of planar topography breaks down at the granular scale and propose a definition of lower-stage plane bed topography that encompasses microforms like bedload sheets, particle clusters, and other low-amplitude bedforms. This definition is appropriate because it is aligned with a hypothesized transition in the processes governing the relief of the bed. It is also aligned with practical considerations related to form roughness, drag partitioning, and preserved sedimentary structures.

Previous studies suggest that particle collisions are important during the initial phase of bedform development. We formalize this idea to propose a quantitative hypothesis that is tested using experimental observations of tracer particle motion over stable and unstable planar topography. Specifically, we hypothesize that quasi-planar topography becomes unstable when the particle collision frequency exceeds the particle entrainment frequency. The dimensionless ratio of these quantities, called the “collision number”, is like an inverse Knudsen number commonly used in fluid physics to quantify the transition from rarefied to continuum transport. We find that the collision number is 0.15 in the stable plane bed experiment and 1.35 in the unstable plane bed experiment despite only a small increase in bed stress, supporting our hypothesis.

Combining empirical and theoretical expressions enables prediction of bed configuration as a function of the macroscopic state variables that govern particle motion. We find that the predicted stability field for microforms is consistent with observations of lower-stage plane bed topography and bedload sheets reported by Carling (1999) and

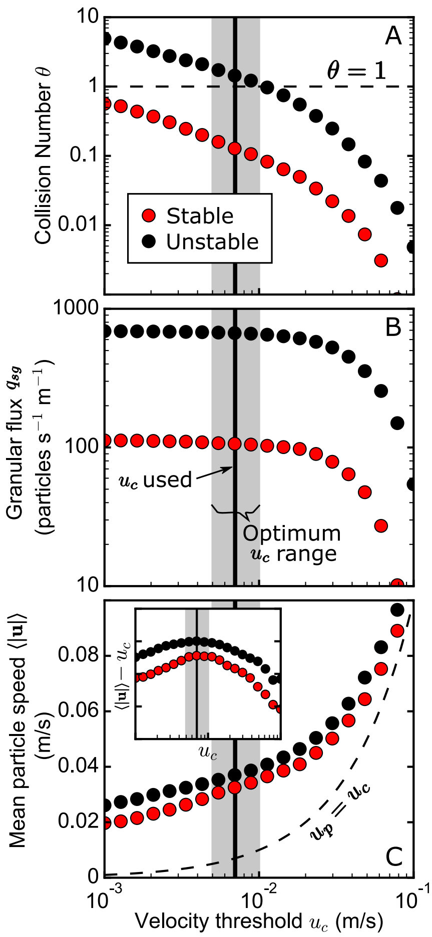

Figure 5. Plot illustrating the effect of the velocity threshold u_c on the measured variables. Although θ is sensitive to the choice of velocity threshold, it varies by an order of magnitude regardless of the specific value used (A). Additionally, measured values straddle $\theta = 1$ within the optimum u_c range. Sediment load is not sensitive to u_c except at very large values because particles that meaningfully contribute to the measured sediment load are ignored (B). We find that the optimum u_c range determined by inspection (Section 5.1) corresponds to the maximum difference between the average measured particle speed and u_c (C).

Guy et al. (1966). Although ripples and dunes have been observed in the region where the collision number is predicted to be less than 1, this may be explained by misclassification of low-amplitude bedforms or uncertainty in measurements of stress. If the overlap is genuine, bed configuration may depend on an additional parameter like the particle Stokes number or Froude number.

In summary, our primary hypotheses represents a coherent synthesis of existing process-based descriptions of bedform initiation focused on various elements of turbulent fluid flow, grain-scale transport, and topographic change. It is supported by experiments reported here and observations of bed configuration reported by previous authors. Three mechanisms are proposed to explain this finding. First, we suggest that grain-scale bed disturbances inevitably self-organize into microforms like bedload sheets, particle clusters, and other low-amplitude bedforms. Second, we suggest that microform amplitude scales with particle diameter and collision frequency. Finally, we suggest that defect propagation and morphodynamic coarsening occurs when microform height exceeds a critical height that is a constant multiple of particle diameter. These mechanisms provide a possible explanation for our results and a starting point for future studies that aim to investigate the mechanisms that determine the stable bed configuration under weak bedload transport conditions.

Acknowledgments

We thank the donors of the American Chemical Society Petroleum Research Fund 54492-DNI8, the National Science Foundation (NSF) grant EAR-1632938, and the University of Wyoming School of Energy Resources for partially supporting this research. We also thank Jelle ten Harkel, Noortje Oosterhoff, and Avelon Gerritsma for assistance with experiments and particle tracking. Data and code are available through Figshare (Ashley, Naqshband, & McElroy, 2020)

References

Abramian, A., Devauchelle, O., Seizilles, G., & Lajeunesse, E. (2019). Boltzmann distribution of sediment transport. *Physical Review Letters*, *123*(1). doi: 10.1103/PhysRevLett.123.014501

Andreotti, B., Claudin, P., & Pouliquen, O. (2010). Measurements of the aeolian sand transport saturation length. *Geomorphology*, *123*(3-4), 343–348. doi: 10.1016/j.geomorph.2010.08.002

Ashley, T. C., Mahon, R. C., Naqshband, S., Leary, K. C. P., & McElroy, B. (2020). Probability distributions of particle hop distance and travel time over equilibrium mobile bedforms. *Journal of Geophysical Research: Earth Surface*, *125*(7). doi: 10.1029/2020JF005647

Ashley, T. C., Naqshband, S., & McElroy, B. J. (2020). Data and code for "Particle collisions control stable bed configuration under weak bedload transport conditions". *Figshare Dataset*. doi: 10.6084/m9.figshare.12475865.v2

Baas, J. H., Best, J. L., & Peakall, J. (2016). Predicting bedforms and primary current stratification in cohesive mixtures of mud and sand. *Journal of the Geological Society*, *173*(1), 12–45. doi: 10.1144/jgs2015-024

Bagherimiyab, F., & Lemmin, U. (2013). Shear velocity estimates in rough-bed open-channel flow. *Earth Surface Processes and Landforms*, *38*(14), 1714–1724. doi: 10.1002/esp.3421

Bagnold, R. A. (1935). The movement of desert sand. *Proceedings of the Royal Society of London. Series A - Mathematical and Physical Sciences*, *157*(892), 594–620. doi: 10.1098/rspa.1936.0218

Ballio, F., Pokrajac, D., Radice, A., & Hosseini Sadabadi, S. A. (2018). Lagrangian and Eulerian description of bed load transport. *Journal of Geophysical Research: Earth Surface*, *123*(2), 384–408. doi: 10.1002/2016JF004087

Best, J. L. (1992). On the entrainment of sediment and initiation of bed defects: insights from recent developments within turbulent boundary layer research. *Sedimentology*, *39*(5), 797–811. doi: 10.1111/j.1365-3091.1992.tb02154.x

Best, J. L. (1996). The fluid dynamics of small-scale alluvial bedforms. In P. A. Carling & M. R. Dawson (Eds.), *Advances in fluvial dynamics and stratigraphy* (pp. 67–125). Manchester, United Kingdom: John Wiley and Sons.

Best, J. L. (2005). The fluid dynamics of river dunes: A review and some future research directions. *Journal of Geophysical Research: Earth Surface*, *110*(F4). doi: 10.1029/2004JF000218

Bialik, R. J. (2011). Particle-particle collision in Lagrangian modelling of saltating grains. *Journal of Hydraulic Research*, *49*(1), 23–31. doi: 10.1080/00221686.2010.543778

Bradski, G. (2000). The OpenCV library. *Dr. Dobb's Journal of Software Tools*, *25*.

Brownlie, W. R. (1981). *Prediction of flow depth and sediment discharge in open channels* (Tech. Rep. No. 43A). Pasadena, California: W. M. Keck Laboratory of Hydraulics and Water Resources, California Institute of Technology.

Carling, P. A. (1999). Subaqueous gravel dunes. *Journal of Sedimentary Research*, *69*(3), 534–545. doi: 10.2110/jsr.69.534

Carling, P. A., Richardson, K., & Ikeda, H. (2005). A flume experiment on the development of subaqueous fine-gravel dunes from a lower-stage plane bed. *Journal of Geophysical Research: Earth Surface*, *110*(F4). doi: 10.1029/2004JF000205

Charru, F., Andreotti, B., & Claudin, P. (2013). Sand ripples and dunes. *Annual Review of Fluid Mechanics*, *45*(1), 469–493. doi: 10.1146/annurev-fluid-011212-140806

Clifford, N. J., Robert, A., & Richards, K. S. (1992). Estimation of flow resistance in gravel-bedded rivers: A physical explanation of the multiplier of roughness length. *Earth Surface Processes and Landforms*, *17*(2), 111–126. doi: 10.1002/esp.3290170202

Coleman, S. E., & Eling, B. (2000). Sand wavelets in laminar open-channel flows. *Journal of Hydraulic Research*, *38*(5), 331–338. doi: 10.1080/00221680009498314

Coleman, S. E., & Melville, B. W. (1994). Bed-form development. *Journal of Hydraulic Engineering*, *120*(5), 544–560. doi: 10.1061/(ASCE)0733-9429(1994)120:5(544)

Coleman, S. E., & Melville, B. W. (1996). Initiation of bed forms on a flat sand bed. *Journal of Hydraulic Engineering*, *122*(6), 301–309. doi: 10.1061/(asce)0733-9429(1996)122:6(301)

Coleman, S. E., & Nikora, V. I. (2009). Bed and flow dynamics leading to sediment-wave initiation. *Water Resources Research*, *45*(4), 1–12. doi: 10.1029/2007WR006741

Coleman, S. E., & Nikora, V. I. (2011). Fluvial dunes: Initiation, characterization, flow structure. *Earth Surface Processes and Landforms*, *36*(1), 39–57. doi: 10.1002/esp.2096

Costello, W. R. (1974). *Development of bed configurations in coarse sands* (Ph.D. Dissertation). Massachusetts Institute of Technology.

Costello, W. R., & Southard, J. B. (1981). Flume experiments on lower-flow-regime bed forms in coarse sand. *SEPM Journal of Sedimentary Research*, *51*(3), 849–864. doi: 10.1306/212F7DC4-2B24-11D7-8648000102C1865D

Dade, W. B., & Friend, P. F. (1998). Grain size, sediment-transport regime and channel slope in alluvial rivers. *Journal of Geology*, *106*(6), 661–675.

Dunne, K. B., & Jerolmack, D. J. (2018). Evidence of, and a proposed explanation for, bimodal transport states in alluvial rivers. *Earth Surface Dynamics*, *6*, 583–594. doi: 10.5194/esurf-6-583-2018

Eaton, B. C., Church, M., & Millar, R. G. (2004). Rational regime model of alluvial channel morphology and response. *Earth Surface Processes and Landforms*, *29*(4), 511–529. doi: 10.1002/esp.1062

Einstein, H. A. (1950). The bed-load function for sediment transportation in open channel flows. *U.S. Department of Agriculture Technical Bulletin 1026*.

Engelund, F., & Fredsoe, J. (1982). Sediment ripples and dunes. *Annual Review of Fluid Mechanics*, *14*(1), 13–37. doi: 10.1146/annurev.fl.14.010182.000305

Engelund, F., & Hansen, E. (1967). *A monograph on sediment transport in alluvial streams* (Tech. Rep.). Technical University of Denmark. doi: 10.1007/s13398-014-0173-7.2

Fathel, S., Furbish, D. J., & Schmeeckle, M. W. (2015). Experimental evidence of statistical ensemble behavior in bed load sediment transport. *Journal of Geophysical Research: Earth Surface*, *120*(11), 2298–2317. doi: 10.1002/2015JF003552

Ferguson, R. I., & Church, M. (2004). A simple universal equation for grain settling velocity. *Journal of Sedimentary Research*, *74*(6), 933–937. doi: 10.1306/051204740933

Fredsoe, J. (1982). Shape and dimensions of stationary dunes in rivers. *Journal of the Hydraulics Division of the American Society of Civil Engineers*, *108*(8), 932–947.

Furbish, D. J. (1997). *Fluid physics in geology: An introduction to fluid motions on Earth's surface and within its crust.* New York: Oxford University Press.

Furbish, D. J., Ball, A. E., & Schmeeckle, M. W. (2012). A probabilistic description of the bed load sediment flux: 4. Fickian diffusion at low transport rates. *Journal of Geophysical Research: Earth Surface*, *117*(F3). doi: 10.1029/2012JF002356

Furbish, D. J., Fathel, S. L., Schmeeckle, M. W., Jerolmack, D. J., & Schumer, R. (2017). The elements and richness of particle diffusion during sediment transport at small timescales. *Earth Surface Processes and Landforms*, *42*(1), 214–237. doi: 10.1002/esp.4084

Furbish, D. J., Haff, P. K., Roseberry, J. C., & Schmeeckle, M. W. (2012). A probabilistic description of the bed load sediment flux: 1. Theory. *Journal of Geophysical Research: Earth Surface*, *117*(F3). doi: 10.1029/2012JF002352

Furbish, D. J., & Schmeeckle, M. W. (2013). A probabilistic derivation of the exponential-like distribution of bed load particle velocities. *Water Resources Research*, *49*(3), 1537–1551. doi: 10.1002/wrcr.20074

Furbish, D. J., Schmeeckle, M. W., Schumer, R., & Fathel, S. L. (2016). Probability distributions of bed load particle velocities, accelerations, hop distances, and travel times informed by Jaynes's principle of maximum entropy. *Journal of Geophysical Research: Earth Surface*, *121*(7), 1373–1390. doi: 10.1002/2016JF003833

García, M. H. (2008). Sediment transport and morphodynamics. In *Sedimentation engineering* (pp. 21–163). Reston, VA: American Society of Civil Engineers. doi: 10.1061/9780784408148.ch02

Gomez, B., Naff, R. L., & Hubbell, D. W. (1989). Temporal variations in bedload transport rates associated with the migration of bedforms. *Earth Surface Processes and Landforms*, *14*(2), 135–156. doi: 10.1002/esp.3290140205

González, C., Richter, D. H., Bolster, D., Bateman, S., Calantoni, J., & Escauriaza, C. (2017). Characterization of bedload intermittency near the threshold of motion using a Lagrangian sediment transport model. *Environmental Fluid Mechanics*, *17*(1), 111–137. doi: 10.1007/s10652-016-9476-x

Guy, H., Simons, D. B., & Richardson, E. (1966). Summary of alluvial channel data from flume experiments, 1956-61. *U.S. Geology Survey Professional Paper 462-I*.

Gyr, A., & Kinzelbach, W. (2004). Bed forms in turbulent channel flow. *Applied Mechanics Reviews*, *57*(1), 77–93. doi: 10.1115/1.1584063

Gyr, A., & Schmid, A. (1989). The different ripple formation mechanisms. *Journal of Hydraulic Research*, *27*(1), 61–74. doi: 10.1080/00221688909499244

Hosseini-Sadabadi, S. A., Radice, A., & Ballio, F. (2019). On reasons of the scatter of literature data for bed-load particle hops. *Water Resources Research*, *55*(2), 1698–1706. doi: 10.1029/2018WR023350

Hubbell, D. W., Stevens, H. H., Skinner, J. V., & Beverage, J. P. (1987). Laboratory data on coarse- sediment transport for bedload-sampler calibrations. *U.S. Geological Survey Water-Supply Paper 2299*.

Ikeda, H. (1983). Experiments on bedload transport, bedforms, and sedimentary structures using fine gravel in the 4-meter-wide flume. *Environmental Research Center Papers, Environmental Research Center, University of Tsukuba*, *2*, 1–78.

Ikeda, S., Parker, G., & Kimura, Y. (1988). Stable width and depth of straight gravel rivers with heterogeneous bed materials. *Water Resources Research*, *24*(5), 713–722. doi: 10.1029/WR024i005p00713

Kahn, D. (1966). Sound propagation in rarefied gases. *Physics of Fluids*, *9*(9), 1867–1869. doi: 10.1063/1.1761948

Kahn, D., & Mintzer, D. (1965). Kinetic theory of sound propagation in rarefied gases. *Physics of Fluids*, *8*(6), 1090–1102. doi: 10.1063/1.1761358

Kauzmann, W. (2012). *Kinetic theory of gases* (2nd ed.). Mineola, New York: Dover Publications, Inc.

Lacey, G. (1930). Stable channels in alluvium. *Minutes of the Proceedings of the Institution of Civil Engineers, Thomas Telford-ICE Virtual Library*, *229*, 259–292.

Lajeunesse, E., Malverti, L., & Charru, F. (2010). Bed load transport in turbulent flow at the grain scale: Experiments and modeling. *Journal of Geophysical Research: Earth Surface*, *115*(4). doi: 10.1029/2009JF001628

Langbein, W. B., & Leopold, L. B. (1968). River channel bars and dunes - Theory of kinematic waves. *U.S. Geological Survey Professional Paper 422-L*.

Leary, K. C. P., & Ganti, V. (2020). Preserved fluvial cross strata record bedform disequilibrium dynamics. *Geophysical Research Letters*, *47*(2). doi: 10.1029/2019GL085910

Leary, K. C. P., & Schmeeckle, M. W. (2017). The importance of splat events to the spatiotemporal structure of near-bed fluid velocity and bedload motion over bedforms: Laboratory experiments downstream of a backward-facing step. *Journal of Geophysical Research: Earth Surface*. doi: 10.1002/2016JF004072

Leclair, S. F., & Bridge, J. S. (2001). Quantitative interpretation of sedimentary structures formed by river dunes. *SEPM Journal of Sedimentary Research*, *71*(2), 713–716. doi: 10.1306/D4268D79-2B26-11D7-8648000102C1865D

Leeder, M. R. (1980). Discussion of the stability of lower stage plane beds and the absence of current ripples in coarse sands. *Journal of the Geological Society*, *138*(6), 753–754. doi: 10.1144/gsjgs.138.6.0753

Liu, M. X., Pelosi, A., & Guala, M. (2019). A statistical description of particle motion and rest regimes in open-channel flows under low bedload transport. *Journal of Geophysical Research: Earth Surface*, *124*(11), 2666–2688. doi: 10.1029/2019JF005140

Mahon, R. C., & McElroy, B. (2018). Indirect estimation of bedload flux from modern sand-bed rivers and ancient fluvial strata. *Geology*, *46*(7), 579–582. doi: 10.1130/G40161.1

Marshall, J. S. (2011). Viscous damping force during head-on collision of two spherical particles. *Physics of Fluids*, *23*(1), 013305. doi: 10.1063/1.3546094

McLean, S. R. (1990). The stability of ripples and dunes. *Earth-Science Reviews*, *29*(1-4), 131–144. doi: 10.1016/0012-8252(0)90032-Q

Métivier, F., Lajeunesse, E., & Devauchelle, O. (2017). Laboratory rivers: Lacey's law, threshold theory, and channel stability. *Earth Surface Dynamics*, *5*, 187–

198. doi: 10.5194/esurf-5-187-2017

Naqshband, S., McElroy, B., & Mahon, R. C. (2017). Validating a universal model of particle transport lengths with laboratory measurements of suspended grain motions. *Water Resources Research*, *53*(5), 4106–4123. doi: 10.1002/2016WR020024

Pähtz, T., Clark, A. H., Valyrakis, M., & Durán, O. (2020). The physics of sediment transport initiation, cessation, and entrainment across aeolian and fluvial nvironments. *Reviews of Geophysics*, *58*(1). doi: 10.1029/2019RG000679

Paola, C., & Borgman, L. (1991). Reconstructing random topography from preserved stratification. *Sedimentology*, *38*(4), 553–565. doi: 10.1111/j.1365-3091.1991.tb01008.x

Parker, G., Wilcock, P. R., Paola, C., Dietrich, W. E., & Pitlick, J. (2007). Physical basis for quasi-universal relations describing bankfull hydraulic geometry of single-thread gravel bed rivers. *Journal of Geophysical Research*, *112*(F4), F04005. doi: 10.1029/2006JF000549

Rapp, B. E. (2017). Fluids. In *Microfluidics: Modelling, mechanics and mathematics* (pp. 243–263). Oxford, UK: Elsevier. doi: 10.1016/B978-1-4557-3141-1.50009-5

Raudkivi, A. J. (1963). Study of sediment ripple formation. *Journal of the Hydraulic Divivision of the American Society of Civil Engineers*, *89*(6), 15–34.

Raudkivi, A. J. (1966). Bed forms in alluvial channels. *Journal of Fluid Mechanics*, *26*(3), 507–514. doi: 10.1017/S0022112066001356

Schindelin, J., Arganda-Carreras, I., Frise, E., Kaynig, V., Longair, M., Pietzsch, T., ... Cardona, A. (2012). Fiji: an open-source platform for biological-image analysis. *Nature Methods*, *9*(7), 676–682. doi: 10.1038/nmeth.2019

Schmeeckle, M. W., Nelson, J. M., Pitlick, J., & Bennett, J. P. (2001). Interparticle collision of natural sediment grains in water. *Water Resources Research*, *37*(9), 2377–2391. doi: 10.1029/2001WR000531

Schumm, S. (1960). The shape of alluvial channels in relation to sediment type. *U.S. Geological Survey Professional Paper 352-B*.

Seizilles, G., Lajeunesse, E., Devauchelle, O., & Bak, M. (2014). Cross-stream diffusion in bedload transport. *Physics of Fluids*, *26*(1). doi: 10.1063/1.4861001

Seminara, G., Colombini, M., & Parker, G. (1996). Nearly pure sorting waves and formation of bedload sheets. *Journal of Fluid Mechanics*, *312*, 253–278. doi: 10.1017/S0022112096001991

Shinbrot, T. (1997). Competition between randomizing impacts and inelastic collisions in granular pattern formation. *Nature*, *389*(6651), 574–576. doi: 10.1038/39264

Smith, J. D., & Mclean, S. R. (1977). Spatially averaged flow over a wavy surface. *Journal of Geophysical Research*, *82*(20). doi: 10.1029/JC082i012p01735

Sommerfeld, M. (2001). Validation of a stochastic Lagrangian modelling approach for inter-particle collisions in homogeneous isotropic turbulence. *International Journal of Multiphase Flow*, *27*(10), 1829–1858. doi: 10.1016/S0301-9322(01)00035-0

Southard, J. B., & Boguchwal, L. A. (1990). Bed configurations in steady unidirectional water flows. Part 2. Synthesis of flume data. *Journal of Sedimentary Petrology*, *60*(5), 658–679. doi: 10.1306/212f9241-2b24-11d7-8648000102c1865d

Southard, J. B., & Dingler, J. R. (1971). Flume study of ripple propagation behind mounds on flat sand beds. *Sedimentology*, *16*, 251–263. doi: 10.1111/j.1365-3091.1971.tb00230.x

Strom, K., Papanicolaou, A. N., Evangelopoulos, N., & Odeh, M. (2004). Microforms in gravel bed rivers: Formation, disintegration, and effects on bedload transport. *Journal of Hydraulic Engineering*, *130*(6), 554–567. doi: 10.1061/(ASCE)0733-9429(2004)130:6(554)

Tinevez, J., Perry, N., Schindelin, J., Hoopes, G. M., Reynolds, G. D., Laplantine, E., ... Eliceiri, K. W. (2017). TrackMate: An open and extensible platform for single-particle tracking. *Methods*, *115*, 80–90. doi: 10.1016/j.ymeth.2016.09.016

Townsend, A. A. (1976). *The structure of turbulent shear flow* (2nd ed.). Cambridge, UK: Cambridge University Press.

van den Berg, J. H., & van Gelder, A. (1993). A new bedform stability diagram, with emphasis on the transition of ripples to plane bed in flows over fine sand and silt. In *Alluvial sedimentation* (pp. 11–21). Oxford, UK: Blackwell Publishing Ltd. doi: 10.1002/9781444303995.ch2

van Rijn, L. (1984). Sediment transport, part III: Bed forms and alluvial roughness. *Journal of Hydraulic Engineering*, *110*(12), 1733–1755.

Venditti, J. G., Church, M., & Bennett, S. J. (2005b). On the transition between 2D and 3D dunes. *Sedimentology*, *52*(6), 1343–1359. doi: 10.1111/j.1365-3091.2005.00748.x

Venditti, J. G., Church, M., & Bennett, S. J. (2006). On interfacial instability as a cause of transverse subcritical bed forms. *Water Resources Research*, *42*(7), 1–10. doi: 10.1029/2005WR004346

Venditti, J. G., Church, M. A., & Bennett, S. J. (2005a). Bed form initiation from a flat sand bed. *Journal of Geophysical Research: Earth Surface*, *110*(1), 1–19. doi: 10.1029/2004JF000149

Venditti, J. G., Nelson, P. A., & Dietrich, W. E. (2008). The domain of bedload sheets. *Marine and River Dune Dynamics*, 175–183.

Whiting, P. J., & Dietrich, W. E. (1990). Boundary shear stress and roughness over mobile alluvial beds. *Journal of Hydraulic Engineering*, *116*(12), 1495–1511. doi: 10.1061/(ASCE)0733-9429(1990)116:12(1495)

Whiting, P. J., Dietrich, W. E., Leopold, L. B., Drake, T. G., & Shreve, R. L. (1988). Bedload sheets in heterogeneous sediment. *Geology*, *16*(2), 105–108. doi: 10.1130/0091-7613(1988)016⟨0105:BSIHS⟩2.3.CO;2

Wiberg, P. L., & Smith, J. D. (1989). Model for calculating bed load transport of sediment. *Journal of Hydraulic Engineering*, *115*(1), 101–123. doi: 10.1061/(ASCE)0733-9429(1989)115:1(101)

Wilcock, P. R. (1996). Estimating local bed shear stress from velocity observations. *Water Resources Research*, *32*(11), 3361–3366. doi: 10.1029/96WR02277

Wilkerson, G. V., & Parker, G. (2010). Physical basis for quasi-universal relationships describing bankfull hydraulic geometry of sand-bed rivers. *Journal of Hydraulic Engineering*, *137*(7), 739–753. doi: 10.1061/(ASCE)HY.1943-7900.0000352

Williams, J. J. E., & Crane, R. I. (1983). Particle collision rate in turbulent flow. *International Journal of Multiphase Flow*, *9*(4), 421–435. doi: 10.1016/0301-9322(83)90098-8

Williams, P. B., & Kemp, P. H. (1971). Initiation of ripples on flat sediment beds. *Journal of the Hydraulic Divivision of the American Society of Civil Engineers*, *97*(4), 502–522.

Winterwerp, J. C., & van Kesteren, W. G. M. (2004). Boundary layer flow. In *Introduction to the physics of cohesive sediment in the marine environment* (chap. 2). Amsterdam, The Netherlands: Elsevier.

Wong, M., & Parker, G. (2006). Reanalysis and correction of bed-load relation of Meyer-Peter and Müller using their own database. *Journal of Hydraulic Engineering*, *132*(11), 1159–1168. doi: 10.1061/(ASCE)0733-9429(2006)132:11(1159)

Wright, S. A., & Parker, G. (2004). Flow resistance and suspended load in sand-bed rivers: Simplified stratification model. *Journal of Hydraulic Engineering*, *130*(8), 796–805. doi: 10.1061/(ASCE)0733-9429(2004)130:8(796)